Biocompatible Film-Coating of Magnetic Soft Robots for Mucoadhesive Locomotion

*Chen Wang, Aldona Mzyk, Romana Schirhagl, Sarthak Misra, and Venkatsubramanian Kalpathy Venkiteswaran**

Magnetically-actuated soft robots for medical applications are required to be functional, biocompatible, as well as capable of robust motion inside human organs. In this paper, a ring-shaped magnetic soft robot, with a flexible biopolymeric film coating, capable of motion on mucus-coated surfaces is designed and investigated. The biopolymeric film made from chitosan–glycerol (C–G) solution endows the robot with robust locomotion capabilities on surfaces of diverse geometrical shapes and orientations. By utilizing mucoadhesive locomotion, the robot has the potential to carry out clinical procedures on enclosed mucus-coated tissue surfaces. Material characterization shows that the mucoadhesion increases with the increase of contact times and/ or preload forces. The softness of the C–G film can be adjusted by controlling the concentration of glycerol. The ring-shaped design and magnetization profile decouple the locomotion and functions of the robot. Additionally, the C–G film-coated robot is tested to be biocompatible for a human colorectal adenocarcinoma cell line with epithelial morphology (HT29). The C–G film reduces the negative effects (superoxide generation) of ferromagnetic particles. Three robot functions including pick-and-place, cargo transportation, and liquid capsule release are demonstrated on different surfaces to show the maneuverability, functionality, and potential of implementing clinical procedures through mucoadhesion.

1. Introduction

Untethered small-scale soft robots have been recently demonstrated to have potential to carry out patient-oriented clinical treatments, such as targeted drug delivery and minimally invasive surgery which provide better prognosis for the patients.[1–4] Owing to the advantages of fast response and wireless actuation, magnetic actuation has gained popularity among other actuation methods for small-scale soft robots with respect to medical applications.[5,6] Existing magnetic soft robots are capable of swimming, crawling, rolling and/or jumping motion patterns.[1,7–9] Recent research has focused on improving robot capability through several aspects including multi-functionality, miniaturization, shape-programmability, multimodal locomotion, sensor integration, and biocompatibility.[10–19]

One of the key requirements for the translation of soft robot technologies into the clinic is for the robots to be robustly controlled inside the human body. This necessitates the robots to move reliably on the surfaces of internal organs (which may be inclined, vertical, or inverted surfaces in confined spaces), working against their own gravity, buoyancy, and friction. Several approaches for improving adhesion have been investigated targeting the abovementioned requirements. Inspired by organisms in nature, special structures and materials have been investigated and verified to have the capability of improving adhesion force on dry or wet condition surfaces.[20–22] For instance, directional mushroom-tipped micro fibers inspired by gecko toes have been verified to have strong adhesion and friction on smooth and dry surface.[23] A spider-silk-inspired composite has been reported to have reliable adhesion on wet and cold substrates from 4 to −196 °C.[24] In order to achieve controllable adhesion and detachment for soft robots, an octopus-inspired hydrogel adhesive has been proposed to enhance the stability of robots operation on in vitro biological tissues.[25] Additionally, forces generated by magnetic field gradients have been used to produce tethering forces for adhering soft robots.[26]

The surfaces of many animal/human organs such as oral cavity, gastrointestinal tract, and stomach are covered with mucus, where it is intended to provide lubrication and protection for epithelial cells of organ surfaces.[27] Mucus consists primarily of water (95%) making it a highly hydrated system. The remaining 5% is made up of mucin glycoproteins, lipids, and inorganic salts.[28] Mucin glycoproteins are the most important
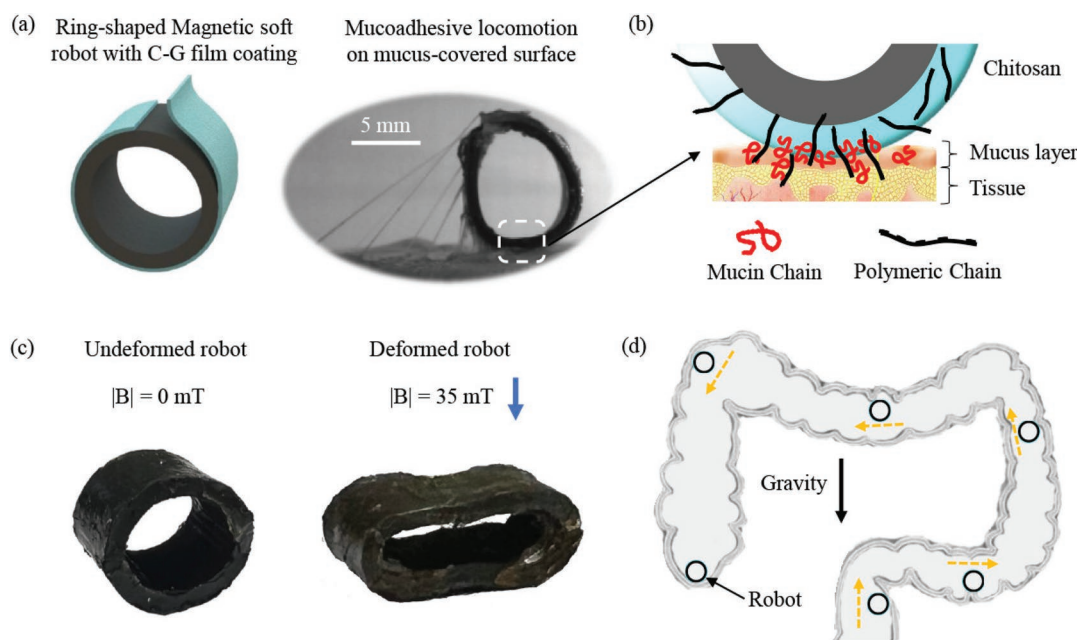
C. Wang, A. Mzyk, R. Schirhagl, S. Misra
Department of Biomedical Engineering
University of Groningen and University Medical Centre Groningen
Groningen 9713 GZ, The Netherlands
S. Misra, V. K. Venkiteswaran
Department of Biomechanical Engineering
University of Twente
Enschede 7500 AE, The Netherlands
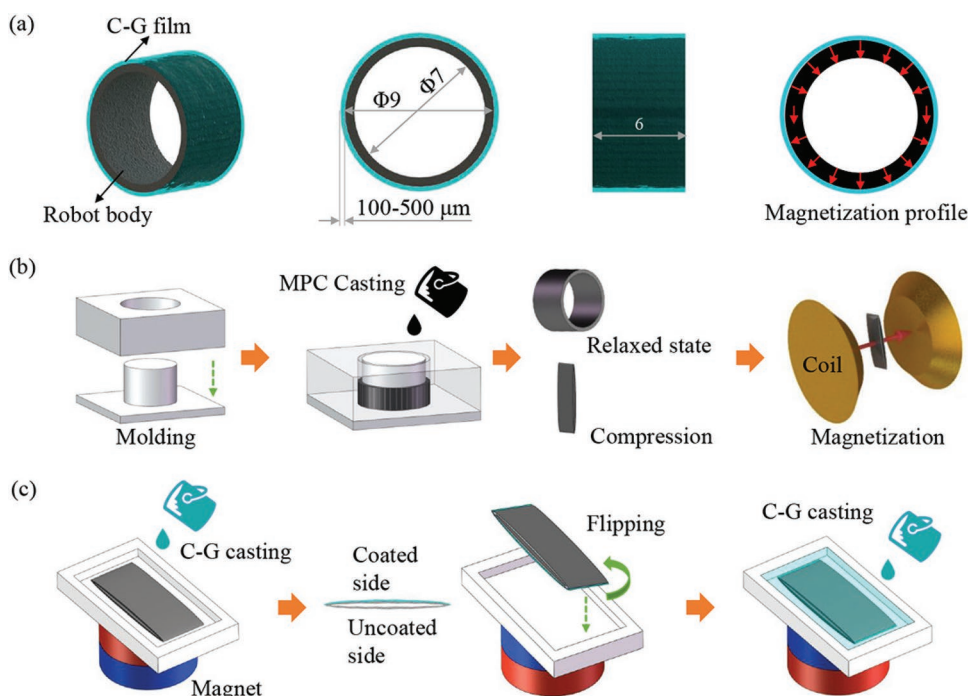E-mail: v.kalpathyvenkiteswaran@utwente.nl

Figure 1. a) Left: 3D model of the ring-shaped magnetic soft robot coated with chitosan–glycerol (C–G) film. Right: video snapshot of the robot rolling on a mucus-coated surface. b) Illustration of polymeric chain in chitosan bonding with mucin chain in mucus. c) The robot locomotion and compression are decoupled by using different magnitudes of the magnetic field. Left: robot maintains its circular shape without magnetic field. Right: the robot is compressed under 35 mT magnetic field. d) Concept of mucoadhesive locomotion of the robot in an enclosed 3D surface (e.g., colon).

structural component of the mucus, resulting in its characteristic gel-like consistency, as well as cohesive and adhesive properties. The thickness and concentration of the mucus layer varies on different mucosal surfaces, from 50 to 450 µm and 3% to 5% in the stomach, to less than 1 µm and 1% in the oral cavity, respectively.[29] Due to its lubricating properties, mucus forms a slippery surface which can be difficult for small-scale soft robots to travel over.

Film coating on the robot surface can ameliorate interaction properties between the robot and mucus. Chitosan is a widely used polymer because it is able to establish various types of mucus interactions with hydrogen bonds and electrostatic interactions to promote adhesion.[30] This is attributed to the interaction of chitosan with sialic acid which is an anionic component present in the mucin. Chitosan presents characteristics including biocompatibility, biodegradability and low toxicity and is a versatile biomaterial used in textile, food industry and medical products. Chitosan has been widely used in drug delivery systems for long-term adhesion on the targeted tissue.[31,32] Recent work has demonstrated the use of chitosan on a soft robot to provide adhesion to tissue surfaces, with the robot able to carry up to 20 times its own weight. The chitosan is applied to the ends of the robot in combination with microfabricated structures which allows for inchworm-like locomotion.[33]

In this paper, the use of a flexible mucoadhesive film-coating on a small-scale soft robot that is actuated by magnetic fields is investigated (shown in **Figure 1**). The motivation of this work is to improve the capability and robustness of robot locomotion on

mucus surfaces and demonstrate potential for mucoadhesion-based medical functions. The use of the C–G soft film coating addresses the challenge of efficient and controllable motion of soft robots while maintaining robust adhesion to mucus-coated surfaces. Compared to previous work, we extend the use of chitosan, using it in combination with glycerol to develop a composite film coating that is flexible and easily applied on soft robot bodies. The locomotion and maneuverability of the robot on surfaces at random tilt angles and of different shape profiles are demonstrated. The robot can also be compressed under an applied magnetic field, and the squeezing action is decoupled from its locomotion. Thus, the robot is also capable of pick-and-place tasks as well as transporting cargo and squeezing a liquid capsule, all under magnetic actuation. The influence of C–G film on the mechanical properties of the robot is evaluated. The mucoadhesive properties of C–G film are characterized through adhesion tests and shear force tests. Additionally, the biocompatibility of C–G film, silicone rubber, magnetic polymer composite (MPC), ferromagnetic particles (FMP) and the C–G film-coated MPC is evaluated based on cell morphology, metabolic activity (MTT assay) and the level of intracellular oxidative stress (T1 relaxometry, DHE assay and DAF-FM assay). The primary contribution of this study is the demonstration of mucoadhesive locomotion in combination with functionality, biocompatibility, and magnetic actuation. Moreover, the development of the soft C–G composite film presented in this paper demonstrates a way to coat the entire external surface of the robot with a biopolymeric film, which may be extended to other soft robots.

ADVANCED
SCIENCE NEWS
www.advancedsciencenews.com

ADVANCED
MATERIALS
TECHNOLOGIES
www.advmattechnol.de

Figure 2. a) Design and dimensions of the magnetic soft ring robot (black inner-ring) with chitosan–glycerol (C–G) coating (blue outer-ring). The magnetic dipoles in the robot are represented by the red arrows. Units not specified in this figure are mm. b) Fabrication and magnetization procedure of the robot. The casting and curing of magnetic polymer composite in the shape of a ring (MPC) are carried out first. The ring is then compressed in a fixture and magnetized between a pair of electromagnetic coils. c) The C–G solution is coated onto the robot in two steps to cover the entire outer surface.

2. Results and Discussion

2.1. Robot Design and Fabrication

The robot is designed for rolling and flipping locomotion under a rotating magnetic field. The robot can also be compressed by increasing the magnitude of the magnetic field in the direction of the initial magnetization. Due to its ring-shaped design and magnetization profile, the locomotion and compression can be decoupled (Figure S1a,b, Supporting Information). Through this decoupling, the robot can be navigated to targeted locations, and the compression (and release) can be used for functional tasks (e.g., controlled release of drugs). The design and dimensions of the ring robot are shown in **Figure 2**a. The inner ring is made of MPC which is responsive to the actuating magnetic field. The directions of magnetic dipoles in the robot body are shown with red arrows. The magnetic dipoles in the robot body are all in the same direction when the robot is compressed to a flat shape. This is achieved by magnetizing the robot in its compressed state.
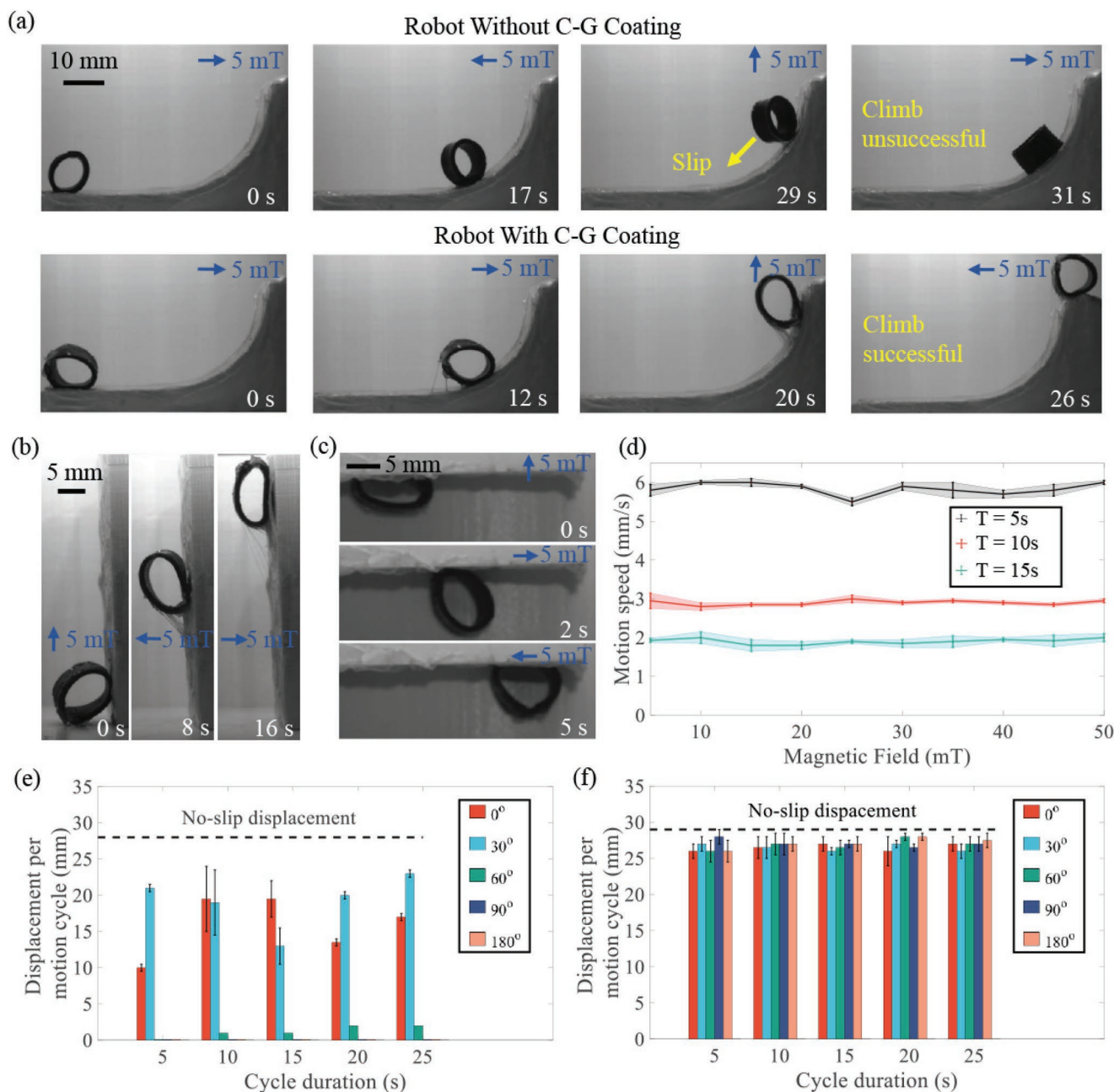
To achieve mucoadhesive locomotion, the outer surface of the ring is coated in a layer of biopolymeric (C–G) film with mucoadhesive properties. The film is soft, smooth, and biocompatible (see Section 2.5 and 2.7). The thickness of the film varies from 100 to 500 μm, depending on the concentrations of the glycerol and the volume of the solution before the formation of film. The polymeric chain in chitosan forms hydrogen bonds with the mucin chain in mucus (shown in Figure 1b), which provides adhesion force for the robot.

The robot body (inner ring) is fabricated using MPC as shown in Figure 2b. Molds are created using laser-cut acrylic (poly-methyl methacrylate) to create the shape of the robot ring. Then, the robot is taken out from the mold and compressed into a flat shape using a fixture. The compressed robot is subjected to a magnetic field of 2 T using an electromagnet to align the magnetic dipoles as shown in Figure 2b. The magnetized ring is then transferred to another mold and kept flattened using an external magnet. The C–G solution is slowly poured into the mold such that it covers the top surface of the robot. After the C–G solution cures, the process is repeated on the other side of the robot as shown in Figure 2c. At the end of the fabrication process, the outer surface of the ring of the robot is fully coated with C–G film.

2.2. Robot Locomotion

To evaluate the mucoadhesive locomotion of C–G film coated robot, a series of setups with different terrains is designed and coated with mucus. A control experiment is carried out to show the capability and advantage of the coated robot compared to its uncoated counterpart when climbing a quarter circle slope against gravity (Movie S1, Supporting Information). As shown in **Figure 3**a, the robot without coating slips and falls down half way up the slope, while the robot with C–G coating moves stably up to the top of the slope. Figure 3b,c show the robot's ability to move on vertical and inverted horizontal surfaces, respectively. As a notable additional observation (Figure 3a),

**ADVANCED
SCIENCE NEWS**

www.advancedsciencenews.com

**ADVANCED
MATERIALS
TECHNOLOGIES**

www.advmattechnol.de

Figure 3. a) Rolling locomotion is achieved by applying a 5 mT rotating magnetic field. The robot without C–G coating is unable to complete the climb up the slope, while the robot with C–G coating completes the climb successfully. b) The robot with C–G coating climbs a vertical (90°) surface. c) The robot with C–G coating rolling on an inverted (180°) surface. d) Robot motion speed under different magnitudes of rotating magnetic field with 5, 10, and 15 s cycle duration on horizontal (0°) surface. e) Displacement per motion cycle of the uncoated robot rolling on 0°, 30°, 60°, 90°, 180° surfaces. f) Displacement per motion cycle of the coated robot rolling on 0°, 30°, 60°, 90°, 180° surfaces. The blue arrows represent the directions of the magnetic field. All motion experiments are performed on mucus-coated surfaces.

the coated robot takes less time than the uncoated one for the same displacement. To explore whether the C–G film coating increases the motion efficiency of the robot further, the displacement per motion cycle of uncoated and coated robot on surfaces with different tilt angles are measured under different cycle durations. Figure 3e,f show the results of uncoated and coated robot, respectively. It can be observed that there is almost no motion on inclines at large angles for the uncoated

robot, while the displacements per motion cycle of coated robot on all angles almost equal the no-slip displacement. The no-slip displacement is calculated theoretically according to the outer diameter of the robot. Additionally, motion speed of the coated robot on a horizontal surface under different magnitudes of magnetic field and different motion cycles are measured. The results shown in Figure 3d illustrate that the magnitudes of the magnetic field do not influence the motion speed of the
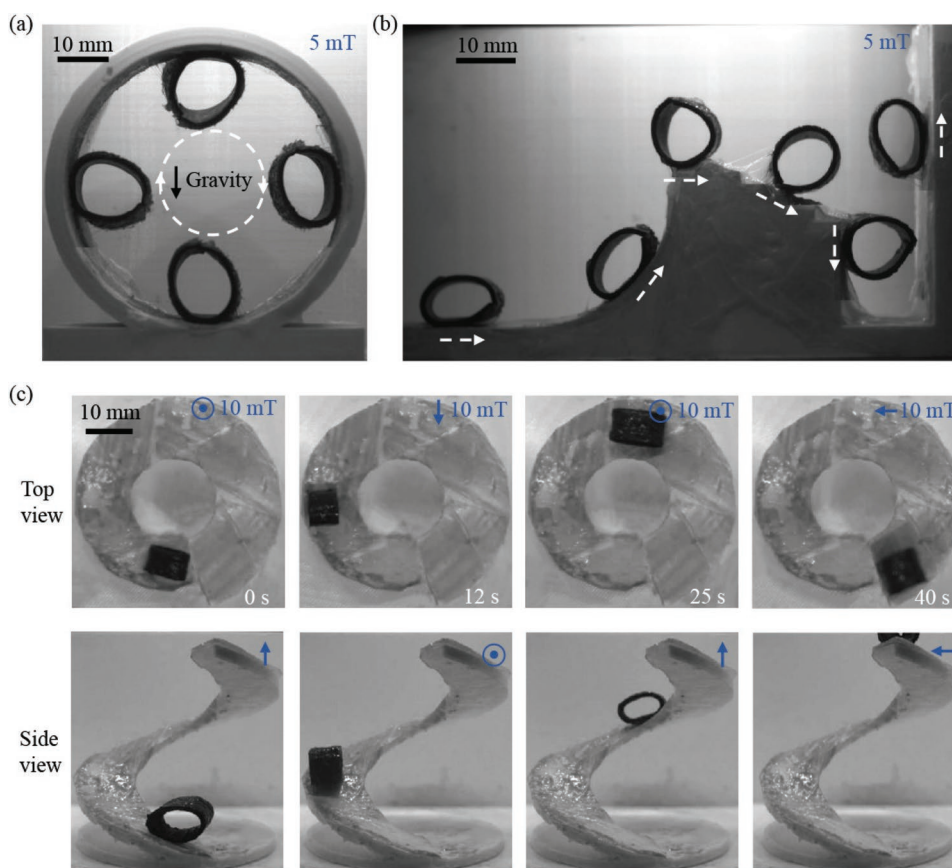
Figure 4. a) Robot rolling on the inner surface of a full circle. b) Robot rolling up a quarter circle slope, down steps, and climbing a vertical wall. c) Robot moving on a spiral upward slope path. The blue arrows represent the directions of the magnetic field.

robot under a certain rotation frequency. The above results indicate that the C–G film on the robot improves the motion efficiency on mucus-coated surface, and improves the capability of moving on surfaces irrespective of their inclinations from the direction of gravity.

2.3. Robot Maneuverability

The robot has the ability to move on mucus-coated surfaces with different 3D shapes (Movie S1, Supporting Information). **Figure 4**a demonstrates the robot rolling in a full circle on the inner surface of a circle, against gravity, under a rotating magnetic field. The magnitude and cycle duration of the rotating magnetic field are 5 mT and 10 s, respectively. The inner diameter of the setup is 35 mm which is around four times the robot outer diameter. Figure 4b shows that the robot rolls up a quarter circle slope, an obstacle (2 mm in height), down steps (2 mm in height and 3 mm in width per step, the final step is 15 mm in height) and climbs a vertical wall in succession without slipping and falling. The magnitude and cycle duration of the rotating magnetic field are 10 mT and 10 s, respectively. Also, the robot has the maneuverability to turn. By changing the tilt angle of the rotating magnetic field plane, the rolling directions of the robot can be changed (shown in Figure S1e, Supporting Information). To demonstrate the steering maneuverability, the

robot is controlled to roll on an upward spiral path as shown in Figure 4c. The path has an inner diameter of 20 and 15 mm width from the top view, and 60 mm height from the side view. The magnitude and cycle duration of the rotating magnetic field are 5 mT and 5 s, respectively.

2.4. Robot Functions

Using the mucoadhesive locomotion, the robot has the ability to reach target locations and implement special functions that are difficult for the robot without coating (Movie S1, Supporting Information). In this paper, three functions, namely pick-and-place, cargo transportation, and liquid capsule release are demonstrated. The function of pick-and-place is demonstrated in the following experiment shown in **Figure 5**a. The robot is first steered to a location where an object is present. The object is a 3D printed blue colored block ($3\times 3 \times3$ mm) made of PLA. The object location is 30 mm higher than the robot's original location. The robot is controlled to climb over the wall and steered to a location beside the object. Then, the robot is controlled to flip over and encircle the object by rotating the actuation magnetic field. By increasing the magnitude of the magnetic field, the robot is compressed to grasp the object. After being flipped back, the robot is navigated to roll to a target location through a downward step. Finally, the object is placed at the target
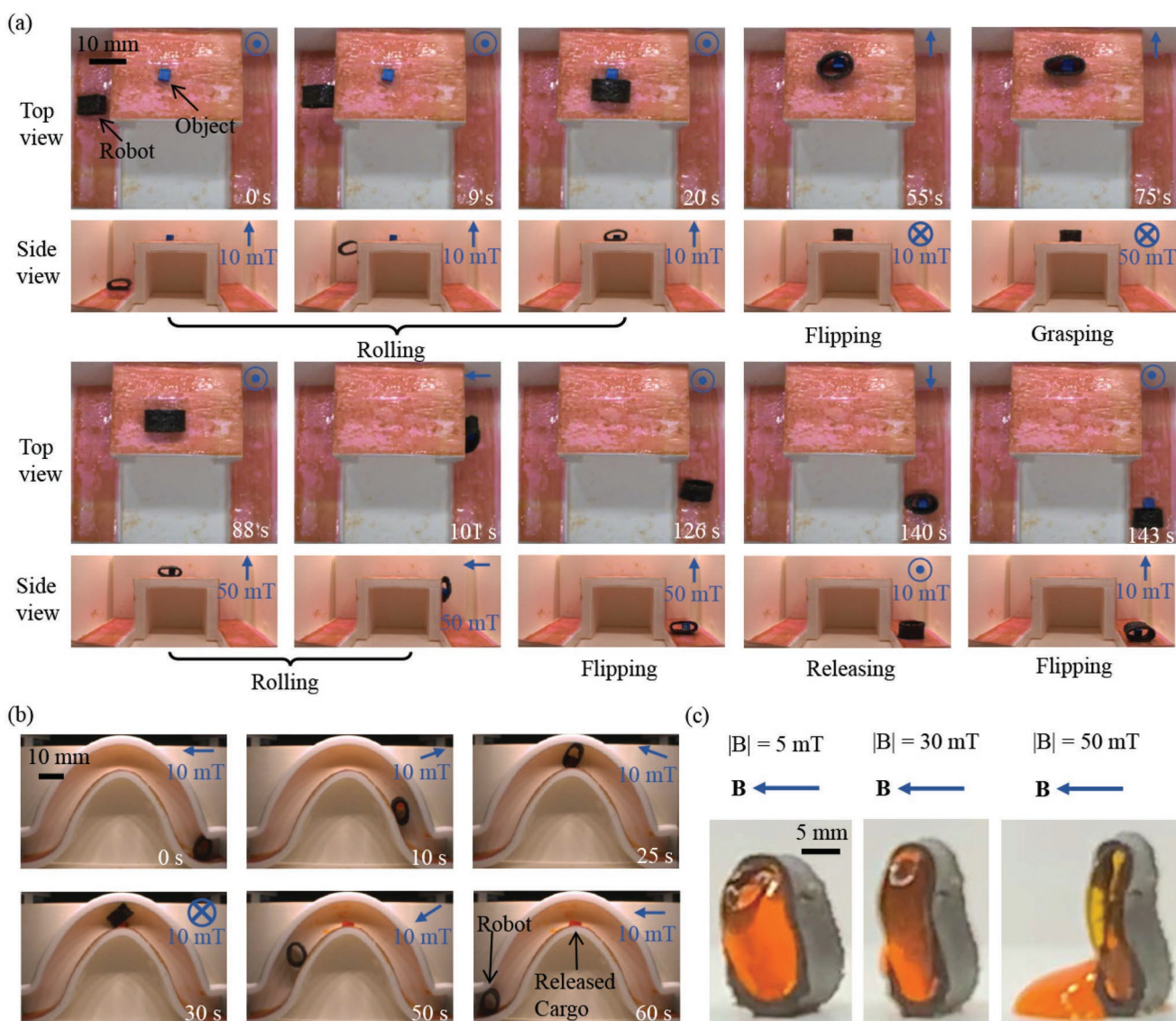
Figure 5. a) Experiment to demonstrate the robot performing pick-and-place operation, where the robot moves a target object between two locations at different elevations. Both the top view and side view are shown. The blue arrows represent the directions of the magnetic field at the given time instant. b) Demonstration of cargo transportation function in a 3D-printed tubular structures. The robot carries a mock-drug up the undulating tube, releases it at the top and subsequently navigates to the bottom. c) The robot demonstrating carrying of a liquid capsule and compression upon magnetic actuation to expel the liquid. The blue arrows represent the directions of the magnetic field.

location by decreasing the magnetic field to restore the robot original shape and flipping the robot.

The robot is also capable of moving through tubular structures and carrying and depositing soft cargo. This is demonstrated in a setup in the shape of an undulating tube with size similar to small intestine. The tube is 3D printed with an inner diameter of 15 mm, and covered with a layer of mucus. The robot is actuated to move up the ascending part of the tube with the soft cargo, tilt to deposit it at the top of the tube and roll down the descent (Figure 5b) (Movie S1, Supporting Information). The magnitude of the magnetic field used during the locomotion is 10 mT. After reaching the target location, the plane of rotating magnetic field changed to flip the robot to unload the cargo.

The robot can also carry and squeeze soft capsules to release liquid contained within as shown in (Figure 5c and Movie S1, Supporting Information). The robot can be compressed by increasing the magnitude of the magnetic field. When the magnetic field reaches 50 mT, the robot is fully compressed, leading to the liquid ball inside being crushed and the liquid in the liquid ball being squeezed out.

2.5. Characterization of Mucoadhesion Properties

To quantitatively analyze the adhesion properties between the C–G film-coated robot and mucus, experiments are designed and carried out to test the adhesion and shear force. The
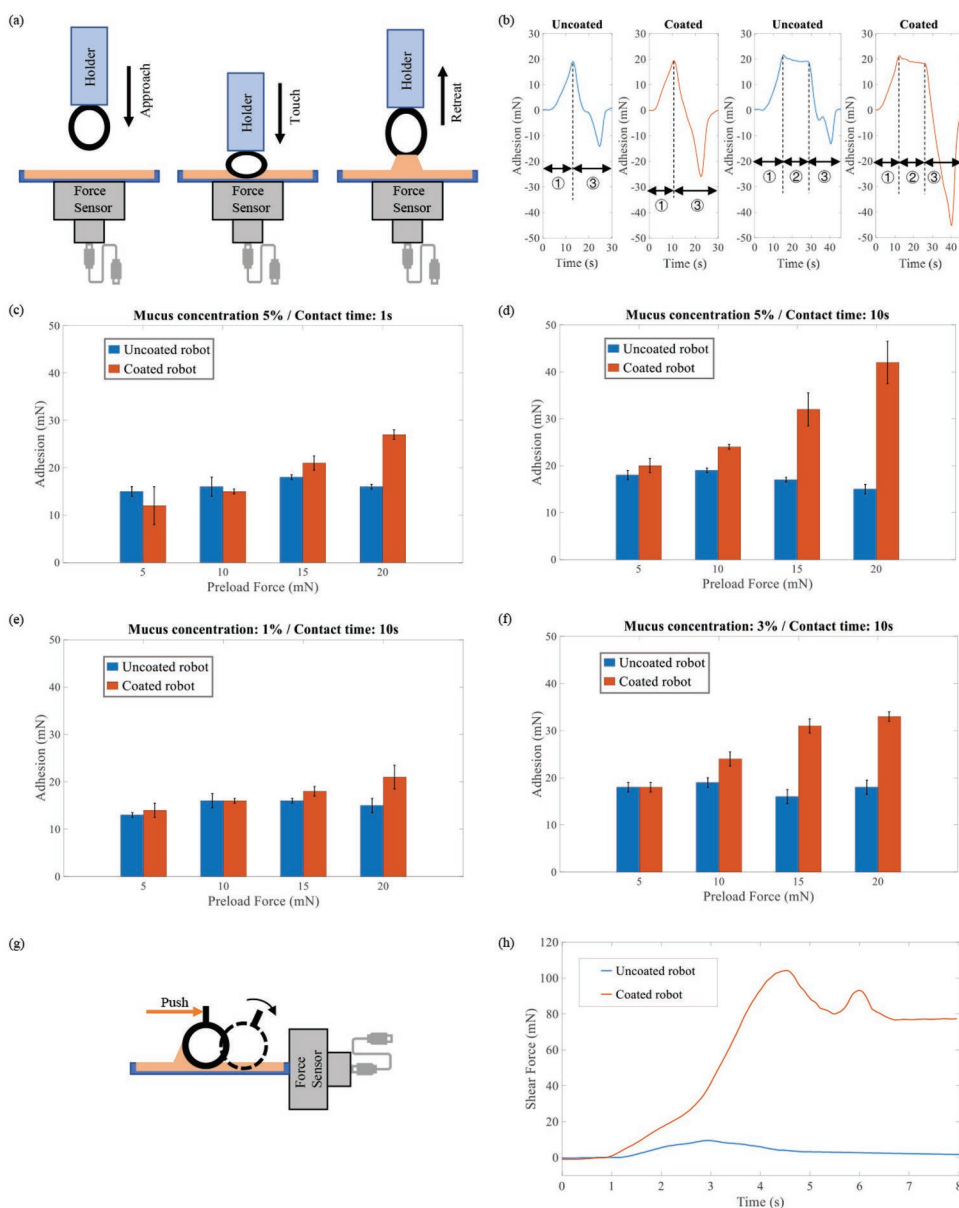
Figure 6. a) Schematics of adhesion force testing: the ring-shaped robot is moved toward the mucus-coated plate to touch the mucus membrane, and then moved away to measure the adhesion force. b) Contact force signal for C–G film-coated and uncoated robots under different contact times, preload force, and contact areas. Stage 1 in the signal refers to the approach phase, stage 2 is the contact phase and stage 3 is the retreat phase. From left to right: the first figure shows the force signal of the uncoated robot with 1 s contact time; the second figure shows the force signal of the coated robot with 1 s contact time; the third figure shows the force signal of the uncoated robot with 10 s contact time; the fourth figure shows the force signal of the coated robot with 10 s contact time. c) Results of adhesion force testing on 5% concentration mucus surface under different contact forces with 1 s contact time. d) Results of adhesion force testing on 5% concentration mucus surface under different contact forces with 10 s contact time. e) Results of adhesion force testing on 1% concentration mucus surface under different contact forces with 10 s contact time. f) Results of adhesion force testing on 3% concentration mucus surface under different contact forces with 10 s contact time. g) Schematic and method for shear force testing. h) Force signal from shear force test over time.

experiment concept and results are shown in **Figure 6**. For testing the adhesion, the robot is held in contact with the mucus plate for different contact times and contact forces (Figure 6a). The results of individual adhesion force tests are shown in Figure 6b. Both coated and uncoated robots are tested. The positive peaks on the signal signify the maximum preload force act between the robot and mucus plate, the negative peaks indicate

the maximum adhesion force generated by the C–G film and mucus. It can be seen from the results that the amplitude of the adhesion of coated robot changes when the contact time increases while there is no noticeable change for the uncoated robot. To explore the influence of preload force under different contact times, two groups of experiments are carried out and the results are shown in Figures 6c and 6d respectively. In

**ADVANCED
SCIENCE NEWS**

www.advancedsciencenews.com

**ADVANCED
MATERIALS
TECHNOLOGIES**

www.advmattechnol.de

Figure 6c, the preload force increases from 5 to 20 mN and the contact time is 1 s. In Figure 6d, the preload force increase from 5 to 20 mN and the contact time is 10 s. The results show that the adhesion force increases with the increase of preload force, and the adhesion force also increases with greater contact time.

In order to test the influence of the concentration of mucus on the adhesion force of robot, mucus-coated surfaces at three different concentrations are prepared. The adhesion forces are measured under different preload forces and 10 s contact time. Figure 6e,f,d shows the results of adhesion force measurement under 1%, 3%, and 5% mucus-coated surfaces, respectively. The results show that the adhesion force of robot increases with the increase of the mucus concentration. It should be noted that the adhesion force of uncoated robot is equal or slightly higher than the coated robot in some cases when the contact time is short and the preload force is low. For the coated robot, the robot locomotion could be more stable by either increasing the contact time or the preload force to magnify the adhesion force. The purpose of this experiment is to explore the trend of adhesion force with the changes of the two factors (contact time and preload force), and compare the results of C–G film-coated robot with the uncoated robot. The results reveal that there is no increasing trend for the uncoated robot while changing the contact time and preload force, whereas the adhesion force of the coated robot changes significantly with the change of the two factors. By using these two factors, the C–G coated robot has potential for controllable locomotion.

The C–G film coated on the robot also affects the friction coefficient. An experiment is designed to measure the shear force during robot locomotion as shown in Figure 6e. The coated and uncoated robot are placed on the mucus plate and pushed with a probe to rotate by 30°. The horizontal force (shear force) is measured by the force sensor. The results in Figure 6f depict that there is a significant increase in the shear force when the robot is coated with the C–G film. Also, the shear force of coated robot remains high after a motion cycle, whereas the shear force of uncoated robot decreases significantly after a motion cycle due to the lubricating action of mucus.

The results of characterization of mucoadhesive properties support the film coating concept. Two factors influence the adhesion and friction between the robot and mucus: contact time and preload force. The results suggest that the increase of the two factors lead to the increase of the adhesion and friction. Thus the adhesion and friction have potential to be controlled for different adhesion requirements. During locomotion, a suitable magnitude and frequency of the rotating magnetic field need to be selected to ensure the locomotion performance of

the robot. In some cases, for instance, the concentrations of the mucus differ depending on locations inside the human body, such as the gastrointestinal tract and stomach. A higher magnetic torque and rolling speed can be used to overcome higher adhesion force, while a lower rolling speed and higher preload force are capable of increasing the adhesion force. Additionally, the adhesion and friction can be improved through microarchitectured structures on the surface of the robot.[23,33]

2.6. Characterization of C–G Films

The tensile modulus of pure chitosan film without glycerol is much higher than the tensile modulus of the robot. Without softening the film is too stiff to go on the robot, meaning that the film will break off when the robot deforms. The deformation of the robot shape is essential for motion and the demonstrated functions. To this end, glycerol is added as plasticizer to the chitosan film. The concentration of glycerol in the C–G film affects its mechanical properties. In order to study the changes in the mechanical properties of the film, different concentrations of glycerol are added to the chitosan solution. The mechanical properties of commercial product Ecoflex 00-10 are used as reference. It can be seen in **Table 1** that the softness and flexibility of the film are higher with increase in the concentration of glycerol. Adding glycerol will affect the concentration of the chitosan which is the main component responsible for mucoadhesion.[31] However, in this paper the changes in concentration of glycerol are minor compared to other studies[34–36] since the focus is on obtaining a suitable recipe that matches the mechanical properties of the film with that of the robot. Based on the results in Table 1, the plasticized chitosan film with 10% glycerol is used for coating the robot.

To explore the influence of C–G film coating on the robot mechanical properties, the deformations of coated and uncoated robot are measured under different magnitudes of magnetic field and external forces (**Figure 7**a). The deformation is measured as a percentage of change in inner diameter to the original inner diameter of the robot. It can be seen in Figure 7b that the deformation percentage increases with the increase of magnetic field, and the coated robot deforms less than the uncoated counterparts. The relationship between the deformation and external force is studied using a compression tester. The results in Figure 7c illustrate that more deformation requires more force on the robot. Naturally, the thinner robot deforms more than the thicker one, while the thicker robot has potential to provide more grasping force under greater magnetic field. Depending on the applications, the above results

Table 1. Effects of different concentrations of glycerol on mechanical properties of the C–G film.

| Film ingredients	Film thickness	Tensile modulus	Tensile strength	Elongation at break
Ecoflex 00-10	3 mm	55 kPa (100% Modulus)	826 kPa	800%
Chitosan	60 μm	566 MPa	31.38 kPa	3.9%
Chitosan + 5% glycerol	90 μm	1.46 MPa	1.09 kPa	59.2%
Chitosan + 10% glycerol	120 μm	800 kPa	0.65 kPa	77.1%
Chitosan + 20% glycerol	90 μm	280 kPa	1.03 kPa	99.7%
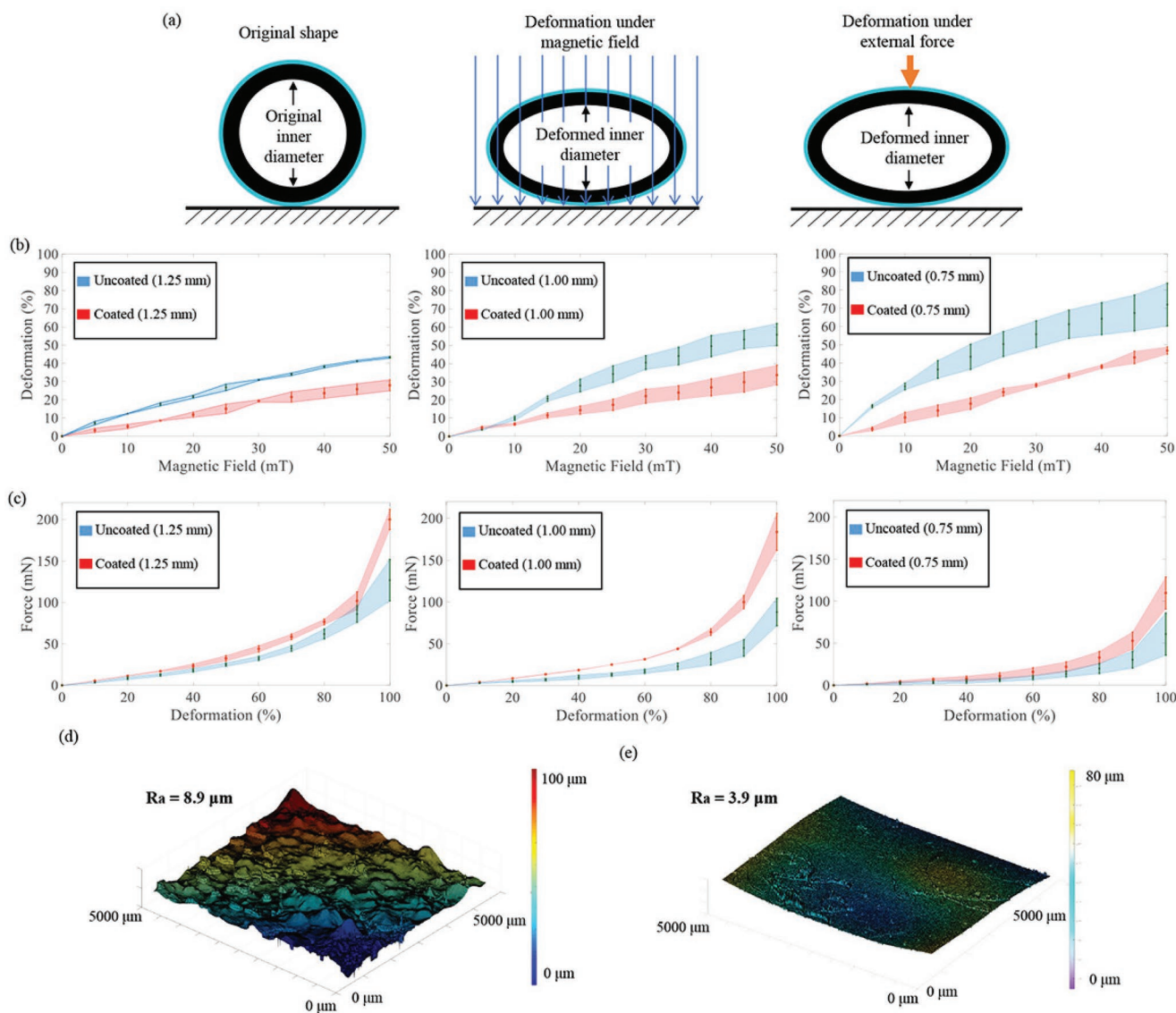
Figure 7. a) Schematics showing deformation of the robot under magnetic field and external force. b) Deformation percentage of the coated and uncoated robot under different magnitudes of the magnetic field. Three thicknesses of the robot are tested: 1.25, 1, and 0.75 mm. c) Force applied on the coated and uncoated robot to achieve different deformations of the robot. Three thicknesses of the robot are tested. d) Surface topography and roughness results of the C–G film by a laser-optical profilometer. e) Surface topography and roughness of the MPC measured by a laser-optical profilometer.

can be taken into account for designing the robot. In addition, the topography and roughness of the surface of the C–G film and MPC are measured using a laser-optical profilometer (Roughness Scantron 2000 Profilometer). The average surface roughness of the C–G film is 8.9 µm as shown in Figure 7d and the average surface roughness of the PMC is 3.9 µm as shown in Figure 7e. Compared to the size of the robot, the C–G film does not significantly alter the roughness of the surface.

2.7. Biocompatibility Tests

Biocompatibility assays are carried out with cells treated for 4 and 24 h with extracts from the materials, since the mean duration of surgeries is 2 h and procedures above 12 h are

rare.[37] Cell morphology results are shown in **Figures 8**a and Figure 8d respectively (full results are shown in Figure S3, Supporting Information). The position of nucleus and distribution of F-actin cytoskeleton fibers within the cells is similar for all sample variants at both analyzed time points. Similarly, the qualitative evaluation of the cell shape and cell–cell interactions indicates lack of significant differences between the specimens. As the change of cell morphology may only in a very limited way reflect the cytotoxic effect of biomaterial, we tested metabolic activity of HT29 cells. The obtained results are shown in Figure S2a,b, Supporting Information. Cells incubated with the suspension of the ferromagnetic particles (FMP) for 4 h are characterized by a higher metabolic activity than the control group. This is only a temporary effect and the metabolic activity of HT29 returns to the level of the control after 24 h.
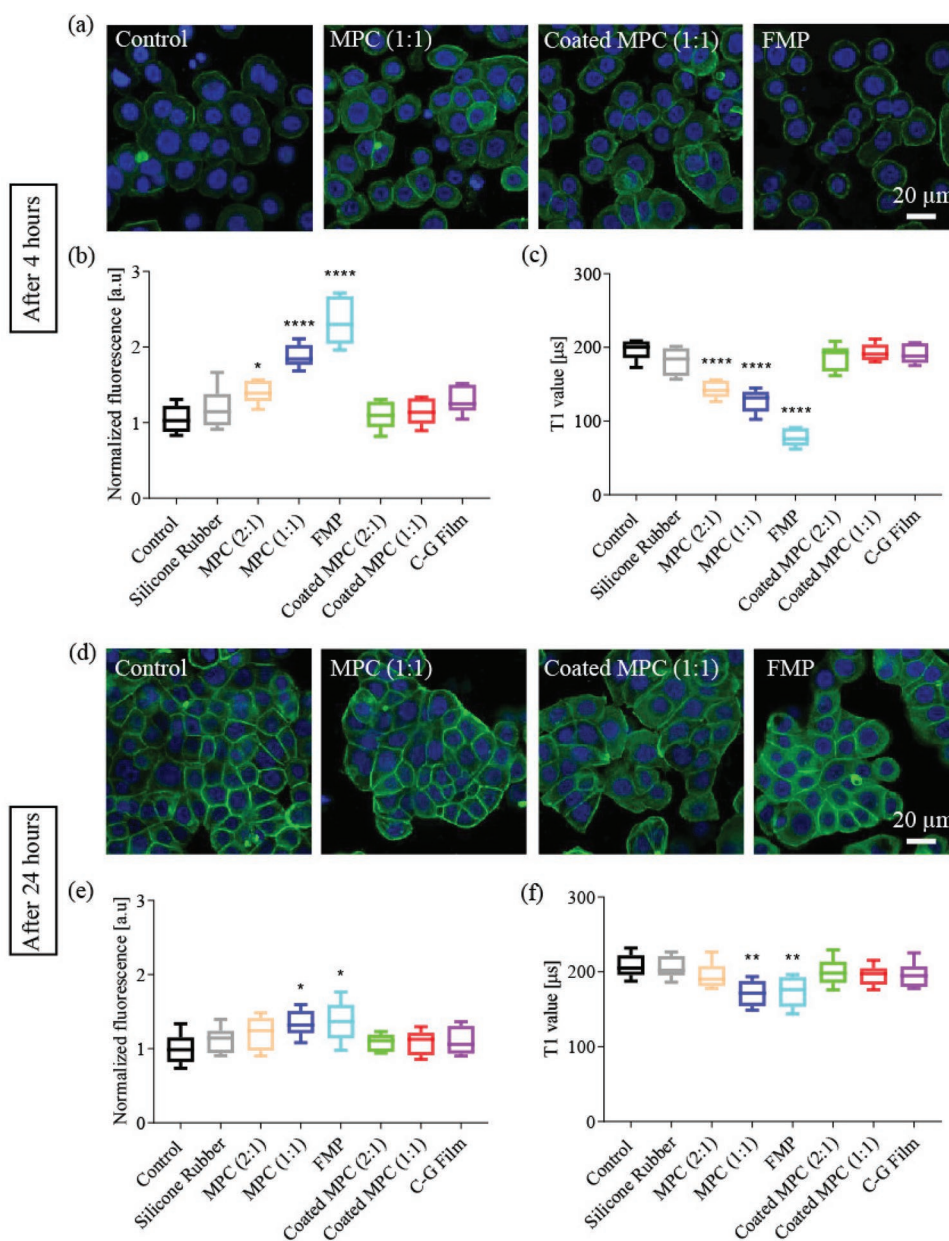
Figure 8. Results of biocompatibility tests. Silicone rubber, magnetic polymer composite (MPC) with 2:1 and 1:1 mass ratio (silicone rubber : magnetic particles), 2 mg mL^{-1} of ferromagnetic particles (FMP), C–G film, and C–G film coated MPC are tested. The results are compared with control group. a) Morphology of the human colorectal adenocarcinoma cell line with epithelial morphology (HT29) after treatment with various material extracts for 4 h. The blue staining (DAPI) indicated nuclei and green (phalloidin Alexa Fluor 488) F-actin filaments of the cytoskeleton. b) Results of dihydroethidium (DHE) assay—detection of intracellular superoxide. Normalized fluorescence calculated for cells treated with various material extracts for 4 h. c) Results of T1 assay—detection of intracellular free radicals. d) HT29 morphology after treatment with various material extracts for 24 h. e) Results of DHE assay—detection of intracellular superoxide. Normalized fluorescence calculated for cells treated with various material extracts for 24 h. f) Results of T1 assay—detection of intracellular free radicals. Positive control—untreated cells. The asterisk signs denote statistical significance (**$p < 0.01$, ***$p < 0.001$, ****$p < 0.0001$) to control groups.

We have not found any significant changes in the metabolic activity of cells after incubation with the other types of extracts. Similarly, we have not found any changes in the intracellular nitric monoxide generation in response to the tested materials (Figure S4a,b, Supporting Information). However, the treatment of the HT29 cells with material extracts increased generation of intracellular superoxide. The results obtained in

DHE assay are shown in Figure 8b,e. It is notable that the concentration of superoxide after 4 h increases with the increase of concentration of FMP, which indicates that the release of FMP from MPC may potentially affect the cells. After 24 h, the concentration of superoxide returns to the level of the control. Similar results were obtained from the T1 relaxometry experiments. The T1 relaxometry allows local detection of the sum

of free radicals, (including reactive oxygen and nitrogen species), within a few tens of nm from a nanodiamond probe. The good agreement of the outcomes of T1 relaxometry and DHE assay indicates clearly that presence of magnetic nanoparticles induces transient oxidative stress in HT29 cells. Rajnbary et al. have shown that magnetic nanoparticles trigger dose-dependent ROS generation in HT29 cells, which results in cell death.[38] We postulate that in our study temporary oxidative stress did not lead to cell apoptosis due to switch on of antioxidant protective system and efficient repair processes. The results also show that coating of MPC with C–G film prevents this undesired cell response. Detailed procedures of discussed assays can be found in Section S2, Supporting Information.

3. Conclusions

In this study, we present a ring-shaped magnetic soft robot that is capable of stable and robust locomotion on mucus-coated surfaces through the use of a biopolymeric adhesive film coating. The efficiency and robustness of motion are improved through C–G film coating compared to the uncoated robot. Our design endows the robot with rolling, flipping and compression capabilities under the control of magnetic field. The robot can perform pick-and-place operations with cargo, as well as carry and squeeze liquid capsules. The C–G film does not lead to a detectable stress response in the form of free radical generation and improves the biocompatibility of the soft robot. The combination of the ring-shaped design, C–G film coating, and magnetic actuation has potential for implementing non-invasive clinical tasks inside the human body.

It is worth noting that the flexible C–G film is not limited to the ring-shaped soft robot presented in this paper. The film can be easily applied on other soft robots due to its flexibility and low surface roughness, for improving mucoadhesion or to reduce cytotoxicity. Moreover, the C–G film is biodegradable.[39] Thus, the film has the potential to load drugs such as brimonidine tartrate[40] and ibuprofen[41] for targeted mucosal drug delivery. The robots can be made fully biocompatible and partially dissolvable by utilizing the C–G film.

Clinical functionalities such as tissue biopsy are also possible, based on the compression and restore actions. However, the force of compression, grasping and restoration need improvement, taking into account the mechanical properties of human tissues.[42,43] Besides increasing the magnitude of magnetic field, various materials such as shape memory polymer[44,45] can be considered for optimizing the action forces. Other wireless actuation methods, such as chemical, temperature and light, can be introduced for actuating the robot to complement the minimalistic motion pattern and the reliable adhesion on the surface. Also, the mucuadhesive locomotion underwater can be investigated. Ex vivo experiments will help validate the efficacy of the film coating. For further development toward clinical applications, soft sensors need to be integrated into the robot for achieving precise location and operation. Other methods such as 3D printing and lithography can help to realize small-scale robot design. If miniaturized, the robots have the potential to broaden the application area to small and narrow spaces such as eyes and urethra inside the human body.

4. Experimental Section

MPC Preparation: The robot is made of a MPC which comprises a silicone rubber matrix (Ecoflex-0010, Smooth-On Inc., USA) and ferromagnetic microparticles (FMP) with a mean particle size of 5 µm (MQFP-16-7-11277, Magnequench GmbH, Germany). The mass ratio of the magnetic microparticles to the silicone rubber was 1:1. The MPC was degassed and then set to cure at room temperature (24 °C) for 4 h. The mechanical properties of the MPC, such as tensile modulus, tensile strength, and elongation at break were characterized and the results can be found in Section 2.7. Additionally, the mechanical properties of silicone rubber were similar to the mechanical properties of biological tissues such as gastrointestinal tract.[42] The robot therefore had potential to be safely used for medical applications in vivo.

C–G Film Preparation: Chitosan was selected as an intermediate medium to form hydrogen bonds with mucin glycoproteins. However, the stiffness of chitosan film was much higher than MPC (10^4 times according to the results from Table 1), which led to the separation of the film from the soft robot body under deformation. To soften the chitosan film, glycerol was chosen as a plasticizer and a composite C–G film was prepared and used in this study. The procedure for preparing the C–G film is as follows: First, chitosan solution (2%, w/v) was prepared by dissolving chitosan powder (medium molecular weight, Sigma-Aldrich, USA) into 1% (v/v) acetic acid solution with a magnetic stirrer for 24 h until the solution is transparent. This was followed by adding glycerol into the chitosan solution and mixing for 1 h. Different concentrations of glycerol (5%, 10%, 20%, w/w) were added to the polymer solutions to observe the influence of glycerol on the mechanical properties of the chitosan film. The obtained solutions were then put into a centrifuge (6000 rpm) for 3 min to remove air bubbles. Finally, the C–G film was obtained by casting C–G solutions on the robot body and drying for 48 h at room temperature.

Mucus Preparation: The motion of the soft robots was to be demonstrated on mucus-coated surface. Pure human mucus was not selected for experiments in this paper as it cannot be stored for long periods of time and varied radically from person to person which decreased the reliability of experiments. Synthetic mucus had the same properties as natural mucus and had advantages such as easy availability and suitability for preparing experiment setups. In this paper, synthetic mucus was prepared and used to mimic the chemical composition of fresh mucus. The mucus was prepared by dissolving synthetic mucin (mucin from porcine stomach, Sigma-Aldrich, USA) into phosphate buffer solution (PBS, pH=7) at concentrations of 1–5% (w/v) and stirring on a magnetic stirrer for 1 h at room temperature (22 °C). The obtained mucus solution was then cast onto silicone rubber film and left to dry at room temperature for 6 h. The liquid thickness of mucus on the silicone rubber film was 1 mm. The dried mucus can be stored in a refrigerator at 8 °C. Before experiments, the dried mucus needed to be sufficiently hydrated by deionized water.[46,47]

Experimental Setup: The liquid capsule (Section 2.4, Figure 5c) was prepared by dropping 2% sodium alginate solution into 1% calcium chloride solution for 5 s. For higher contrast with the background, the mock drug was dyed orange by adding a small quantity of the dye (Sudan Orange color dye, Merck, Germany). The soft cargo used for demonstrating the cargo transportation function reference was made by the same process as the liquid capsule but with more reaction time (1 min) to produce a hydrogel. The setups for demonstrations in this paper were 3D-printed using polylactic acid. The surface of the setup was covered by a thin layer of silicone rubber which was coated with a layer of mucus. Experiments were carried out between 10 and 20 min after hydrating the mucus at room temperature (22 °C).

Mechanical Performance Characterization of C–G Film: Uniaxial tensile tests were carried out to characterize the tensile modulus, tensile strength, and elongation at break of the prepared C–G films with different concentrations of glycerol. The above mechanical properties were measured on a texture analyzer (CT3 Texture Analyzer, USA). The thickness of the films was measured using a custom-built low load compression tester. The mechanical properties of the films are tested

**ADVANCED
SCIENCE NEWS**

www.advancedsciencenews.com

**ADVANCED
MATERIALS
TECHNOLOGIES**

www.advmattechnol.de

by following ASTM D882 and ASTM D412 standards respectively. All the values are average value from three times of test. The results can be found in Section 2.7.

*Characterization of Mucoadhesion Properties:*The adhesion and shear force were measured using a custom setup where a low range load cell was embedded (shown in Figure 6a). The load cell was able to measure force from 1 mN to 10 N. For measuring the adhesion, the robot and mucus plate were mounted on a movable holder and force sensor, respectively. The adhesion was measured by moving the robot to contact the mucus plate. The contact time can be controlled. For measuring the shear force, the sensor was mounted to measure force along the length of the mucus plate. The robot was placed on the mucus plate and pushed by a probe/stylus to rotate by 30°.

*Biocompatibility Tests:*Materials used in this study, including the C–G film, silicone rubber, MPC, C–G film-coated MPC and magnetic microparticles (2 mg mL^{-1} magnetic particles in medium), were tested for their biocompatibility. The MPC was prepared in two variants of mass ratio, 1:1 and 2:1 (silicone rubber:magnetic particles).

For testing biocompatibility of the materials used in fabricating the robots, a human colorectal adenocarcinoma cell line with epithelial morphology (HT29) was used. Cells were cultured in the DMEM high glucose medium that contains 10% FBS and 1% antibiotics at 37 °C with 5% CO$_2$/95% air until 90% confluence. An indirect method for evaluating cytotoxicity of materials was used in this study. Materials for tests were incubated in the cell culturing medium (medium-to-sample area ratio of 1.25 mL cm^{-2}) for 24 h at 37 °C in a humidified atmosphere of 5% CO$_2$ in order to obtain extracts, which potentially contain cytotoxic components such as magnetic particles and derivatives of degraded polymers.

A DHE assay kit, containing a fluorescent probe, was utilized in order to inspect the generation of superoxide (O$_2^{\cdot-}$) in HT29 cells exposed to material extracts. DAF-FM diacetate (4-amino-5-methylamino-2′, 7′-difluorofluorescein diacetate), a fluorescent indicator developed to detect the intracellular nitric monoxide (NO$^\cdot$) was used in order to determine the impact of materials on free radicals generation in cells. T1 measurements allow local detection of the sum of all radicals within a few tens of nm from a nanodiamond particle with a mean hydrodynamic diameter of 70 nm and a flake-like structure (Adamas Nanotechnologies, NC, USA) as probes.[48–52] They were produced by HPHT synthesis and irradiated with 3 MeV electrons at a fluence of 5×10^{19} e cm^{-2} to produce nitrogen vacancy (NV) centers. As a result each particle contained ≈500 NV centers. As a last step of fabrication these particles were treated in oxidizing acids leading to oxygen termination.[53]

Supporting Information

Supporting Information is available from the Wiley Online Library or from the author.

Acknowledgements

Conflict of Interest

The authors declare no conflict of interest.

Data Availability Statement

The data that support the findings of this study are available from the corresponding author upon reasonable request.

[1] W. Hu, G. Z. Lum, M. Mastrangeli, M. Sitti, *Nature* **2018**, *554*, 7690.
[2] M. Eshaghi, M. Ghasemi, K. Khorshidi, *Extreme Mech. Lett.* **2021**, *44*.
[3] C. Majidi, *Adv. Mater. Technol.* **2019**, *4*, 2.
[4] B. J. Nelson, I. K. Kaliakatsos, J. J. Abbott, *Annu. Rev. Biomed. Eng.* **2010**, *12*, 55.
[5] M. Sitti, *Nat. Rev. Mater.* **2018**, *3*, 6.
[6] M. Tonutti, D. S. Elson, G.-Z. Yang, A. W. Darzi, M. H. Sodergren, *Postgrad Med. J.* **2017**, *93*, 1097.
[7] T. Wang, W. Hu, Z. Ren, M. Sitti, *IEEE Rob. Autom. Lett.* **2020**, *5*, 3.
[8] V. K. Venkiteswaran, D. K. Tan, S. Misra, *Extreme Mech. Lett.* **2017**, *93*, 1097.
[9] C. Ahn, X. Liang, S. Cai, *Adv. Mater. Technol.* **2019**, *4*, 7.
[10] H. Deng, K. Sattari, Y. Xie, P. Liao, Z. Yan, J. Lin, *Nat. Commun.* **2020**, *11*, 71.
[11] S. Wu, W. Hu, Q. Ze, M. Sitti, R. Zhao, *Multifunct. Mater.* **2020**, *3*, 4.
[12] V. K. Venkiteswaran, L. P. Samaniego, J. Sikorski, S. Misra, *IEEE Robot. Autom. Lett.* **2019**, *4*, 2.
[13] Y. Kim, H. Yuk, R. Zhao, S. A. Chester, X. Zhao, *Nature* **2018**, *558*, 7709.
[14] J. Zhang, Z. Ren, W. Hu, R. H. Soon, I. C. Yasa, Z. Liu, M. Sitti, *Sci. Robot.* **2021**, *6*, 53.
[15] S. Zhang, Z. Cui, Y. Wang, J. den Toonder, *ACS Appl. Mater. Interfaces* **2021**, *13*, 17.
[16] L. Pancaldi, L. Noseda, A. Dolev, A. Fanelli, D. Ghezzi, A. J. Petruska, M. S. Sakar, *Adv. Intell. Syst.* **2022**, *4*, 2100247.
[17] C. Wang, V. R. Puranam, S. Misra, V. K. Venkiteswaran, *IEEE Robot. Autom. Lett.* **2022**, *7*, 2.
[18] S. Noh, S. Jeon, E. Kim, U. Oh, D. Park, S. H. Park, S. W. Kim, H. Choi, S. Pané, B. J. Nelson, J.-y. Kim, *Small* **2022**, *18*, 2107888.
[19] T. Xu, J. Zhang, M. Salehizadeh, O. Onaizah, E. Diller, *Sci. Rob.* **2019**, *4*, 29.
[20] X. Zhang, G. Chen, Y. Yu, L. Sun, Y. Zhao, *Research* **2020**, *2020*, 3672120.
[21] M. Baby, V. K. Periya, S. K. Sankaranarayanan, S. C. Maniyeri, *Appl. Surf. Sci.* **2020**, *505*, 144414.
[22] X.-C. Li, D.-Z. Hao, W.-J. Hao, X.-L. Guo, L. Jiang, *ACS Appl. Mater. Interfaces* **2020**, *12*, 45.
[23] M. P. Murphy, B. Aksak, M. Sitti, *Small* **2009**, *5*, 2.
[24] L. Xi, L. Shi, X. Wan, B. Dai, M. Yang, Z. Gu, X. Shi, L. Jiang, S. Wang, *Adv. Mater.* **2021**, *33*, 14.
[25] Y. Lee, S. Chun, D. Son, X. Hu, M. Schneider, M. Sitti, *Adv. Mater.* **2022**, *34*, 13.
[26] V. K. Venkiteswaran, S. Misra, in *Proc. of the IEEE/RSJ Int. Conf. on Intelligent Robots and Systems (IROS)*, IEEE, Piscataway, NJ **2020**, pp. 8633–8639.
[27] R. Bansil, B. S. Turner, *Adv. Drug Delivery Rev.* **2018**, *124*.
[28] J. D. Smart, *Adv. Drug Deliv. Rev.* **2005**, *57*, 11.
[29] J. Varshosaz, N. Tavakoli, F. Roozbahani, *Drug Delivery* **2006**, *13*, 4.
[30] M. F. Maitz, *Biosurface and Biotribology* **2015**, *1*, 3.

[31] M. P. C. de Souza, R. M. Sábio, T. de Cassia Ribeiro, A. M. D. Santos, A. B. Meneguin, M. Chorilli, *J. Biol. Macromol.* **2020**, *159*, 804.

[32] L. Sun, J. Sun, L. Chen, P. Niu, X. Yang, Y. Guo, *Carbohydr. Polym.* **2017**, *163*, 81.

[33] Y. Wu, X. Dong, J. kang Kim, C. Wang, M. Sitti, *Sci. Adv.* **2022**, *8*, eabn3431.

[34] C.-M. Lehr, J. A. Bouwstra, E. H. Schacht, H. E. Junginger, *Int. J. Pharm.* **1992**, *78*, 43.

[35] J. F. Fundo, M. A. Quintas, C. L. Silva, in *Proc. of the 11th International Congress on Engineering and Food*, Athens, Greece, May **2011**.

[36] N. E. Suyatma, L. Tighzert, A. Copinet, V. Coma, *J. Agric. Food. Chem.* **2005**, *53*, 10.

[37] A. da Silva Costa, *Einstein (Sao Paulo)* **2017**, *15*, 200.

[38] A. G. Ranjbary, G. K. Saleh, M. Azimi, F. Karimian, J. Mehrzad, J. Zohdi, *Biol. Trace. Elem. Res.* **2022**, *1*, 11.

[39] M. Kammoun, M. Haddar, T. K. Kallel, M. Dammak, A. Sayari, *Int. J. Biol.* **2013**, *5*, 62.

[40] B. Li, J. Wang, Q. Gui, H. Yang, *Bioact. Mater.* **2020**, *5*, 3.

[41] C. Tang, Y.-X. Guan, S.-J. Yao, Z.-Q. Zhu, *Int. J. Pharm.* **2014**, *473*, 434.

[42] J. L. Sparks, N. A. Vavalle, K. E. Kasting, B. Long, M. L. Tanaka, P. A. Sanger, K. Schnell, T. A. Conner-Kerr, *Adv. Skin Wound Care* **2015**, *28*, 2.

[43] P. Li, S. Jiang, Y. Yu, J. Yang, Z. Yang, *J. Mech. Behav. Biomed. Mater.* **2015**, *49*, 220.

[44] B. Jin, H. Song, R. Jiang, J. Song, Q. Zhao, T. Xie, *Sci. Adv.* **2018**, *4*, eaao3865.

[45] A. Lendlein, *Sci. Rob.* **2018**, *3*, 18.

[46] B. T. Burruano, R. L. Schnaare, D. Malamudd, *Contraception* **2002**, *66*, 2.

[47] L. M. Lichtenberger, J. J. Romerod, *J. Gastroenterol. Hepatol.* **1994**, *9*, S1.

[48] L. Nie, A. Nusantara, V. Damle, M. Baranov, M. Chipaux, C. Reyes-San-Martin, T. Hamoh, C. Epperla, M. Guricova, P. Cigler, G. V. D. Bogaart, *Nano Lett.* **2021**, *22*, 4.

[49] N. Norouzi, A. C. Nusantara, Y. Ong, T. Hamoh, L. Nie, A. Morita, Y. Zhang, A. Mzyk, R. Schirhagl, *Carbon* **2022**, *199*, 444.

[50] A. Sigaeva, A. Hochstetter, S. Bouyim, M. Chipaux, M. Stejfova, P. Cigler, R. Schirhagl, *Small* **2022**, *2201395*.

[51] F. P. Martíne, A. C. Nusantara, M. Chipaux, S. K. Padamati, R. Schirhagl, *ACS Sens.* **2020**, *5*, 12.

[52] A. Morita, T. Hamoh, F. P. P. Martinez, M. Chipaux, A. Sigaeva, C. Mignon, K. J. van der Laan, A. Hochstetter, R. Schirhagl, *Nanomaterials* **2020**, *10*, 3.

[53] O. A. Shenderova, A. I. Shames, N. A. Nunn, M. D. Torelli, I. Vlasov, A. Zaitsev, *J. Vac. Sci. Technol. B* **2019**, *37*, 3.